Absolute cross-section measurements for electron-impact ionization of doubly charged ions Ti^{2+}, Fe^{2+}, Ar^{2+}, Cl^{2+}, and F^{2+}

D. W. Mueller, T. J. Morgan,* and G. H. Dunn
Joint Institute for Laboratory Astrophysics, University of Colorado and National Bureau of Standards, Boulder, Colorado 80309

D. C. Gregory and D. H. Crandall†
Physics Division, Oak Ridge National Laboratory, Oak Ridge, Tennessee 37830
(Received 26 December 1984)

Measurements have been made of the cross section for electron-impact single ionization of the ions Ti^{2+}, Fe^{2+}, Ar^{2+}, Cl^{2+}, and F^{2+}, spanning the range of energies from below threshold to 1500 eV. Indirect processes such as excitation-autoionization contribute substantially to the cross section for Ti^{2+}, while such contributions are less pronounced for the other species. Comparisons with available theoretical predictions and with the Lotz semiempirical formula are presented. Expansion coefficients and formulas for generating ionization rate coefficients in the temperature range $10^4 < T < 10^7$ K are included for each ion.

I. INTRODUCTION

Modeled descriptions of the ionization balance in fusion and astrophysical plasmas rely on atomic data to describe the elementary processes. Because no reliable measurements have been made for many cases, the basic data employed must be obtained from theoretical calculations or semiempirical formulas such as the Lotz equation.[1] For ionization these predicted cross sections may differ from reality by more than an order of magnitude,[2] since indirect ionization processes such as excitation-autoionization are not included in the calculation. While direct ionization may be moderately well predicted, the situation for the indirect processes is less clear, as will be demonstrated later in this paper.

Data for species of current importance, particularly for controlled fusion research,[3] are presented here. Measurements have been made of the cross section for electron-impact single ionization of the ions Ti^{2+}, Fe^{2+}, Ar^{2+}, Cl^{2+}, and F^{2+}, spanning the range of energies from below threshold to 1500 eV. By comparing measured cross sections with calculated values, indications of the magnitude of indirect processes are obtained.

In spite of their great importance in both fusion and astrophysical plasmas, no previous experimental data are available for iron ions of any charge state. Similarly, there are no data for any ions of F or Cl. For Ti, only measurements on Ti^{3+} have been reported.[2] Ionization cross sections for the species presented here then serve the dual purpose of direct application to fusion plasmas and of providing information on trends in indirect ionization processes.

II. EXPERIMENTAL DATA

The measurements were conducted using the crossed-beams technique with the apparatus illustrated in Fig. 1. The apparatus and techniques used were similar to those described in detail elsewhere.[4] Target ions were extracted from the ion source, formed into a beam, and led into a region of ultrahigh vacuum ($\sim 10^{-9}$ Torr or 1.3×10^{-7} Pa), where the ion beam crossed an electron beam at 90°. An electrostatic parallel-plate analyzer separated ions of different charge-to-energy ratio, thus separating the primary beam from ions which had undergone ionizing collisions. During measurement periods the primary ions and electron currents, I_i and I_e, respectively, were measured using current integrators, and the product ions were individually counted using a channeltron electron multiplier. Beam profiles for electrons and ions, $R(z)$ and $G(z)$, respectively, were measured and the geometrical overlap F, which has dimensions of length, was determined by

$$F=\frac{\int R(z)dz \int G(z)dz}{\int R(z)G(z)dz} . \quad (1)$$

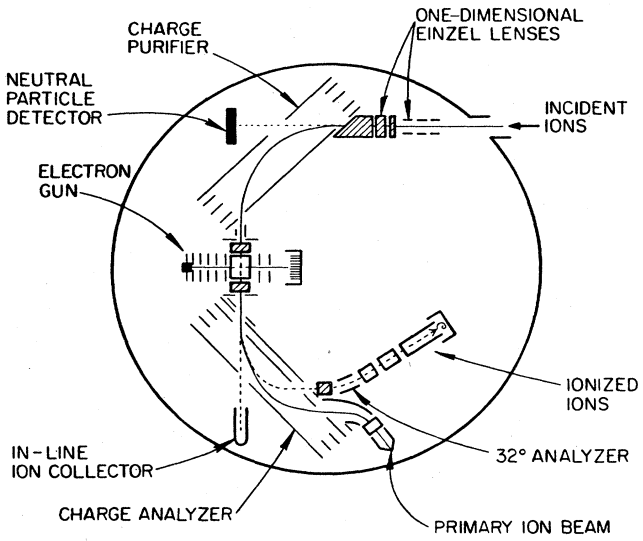

FIG. 1. Crossed-beam collision chamber viewed from above.

 ©1985 The American Physical Society

TABLE I. Measured cross sections for single-electron ionization of F^{2+}, Cl^{2+}, Ar^{2+}, Ti^{2+}, and Fe^{2+} by electron impact. Values in parentheses are one standard deviation of the mean from counting statistics and are taken as representative of relative uncertainties.

Target	E (eV)	σ (10^{-18} cm^2)	Target	E (eV)	σ (10^{-18} cm^2)
F^{2+}	56.2	−0.14(0.14)	Cl^{2+}	70.2	44.44(0.63)
	61.1	0.65(0.11)		71.1	43.60(0.63)
	66.2	2.28(0.14)		72.2	44.18(0.63)
	71.0	5.35(0.17)		74.0	45.43(0.65)
	76.1	6.96(0.27)		76.2	44.15(0.63)
	80.9	8.80(0.21)		78.1	47.27(0.65)
	85.9	9.78(0.36)		80.1	46.54(0.63)
	90.7	10.93(0.24)		80.8	45.99(0.64)
	95.9	11.75(0.14)		86.0	45.32(0.62)
	105.8	13.74(0.28)		90.8	45.27(0.60)
	116.0	14.76(0.17)		95.8	44.64(0.29)
	131.0	16.38(0.16)		100.4	44.00(0.37)
	146.0	17.24(0.61)		105.4	44.25(0.36)
	165.0	17.84(0.14)		110.0	46.09(0.49)
	180.0	18.26(0.15)		115.0	46.55(0.66)
	194.0	18.52(0.11)		120.0	46.16(0.46)
	232.0	17.80(0.15)		144.0	43.00(0.59)
	263.0	17.97(0.14)		174.0	40.17(0.54)
	293.0	17.70(0.13)		213.0	37.31(0.47)
	391.0	16.08(0.14)		253.0	35.24(0.43)
	490.0	14.63(0.10)		292.0	31.98(0.37)
	589.0	13.87(0.09)		390.0	27.13(0.38)
	688.0	12.95(0.06)		489.0	21.69(0.27)
	836.0	11.06(0.09)		687.0	18.25(0.24)
	986.0	10.15(0.08)		885.0	15.48(0.22)
	1184.0	8.95(0.07)		1181.0	12.25(0.15)
	1481.0	7.71(0.09)		1477.0	10.65(0.17)
Cl^{2+}	31.2	0.19(0.61)	Ar^{2+}	15.9	0.32(0.19)
	36.3	−0.07(0.47)		20.8	0.86(0.21)
	38.4	2.78(0.53)		25.7	2.17(0.21)
	40.5	6.85(0.51)		30.8	3.65(0.18)
	41.1	7.91(0.91)		35.7	4.30(0.18)
	42.2	12.89(0.54)		40.7	8.34(0.19)
	43.2	18.33(0.65)		45.5	24.52(0.21)
	44.2	21.64(0.57)		50.5	34.49(0.18)
	45.1	24.68(1.06)		55.3	39.59(0.18)
	46.3	28.30(0.44)		65.3	44.47(0.18)
	46.9	29.13(0.61)		75.1	48.50(0.18)
	48.3	30.18(0.59)		85.0	49.46(0.18)
	49.0	32.06(0.75)		95.0	46.62(0.09)
	50.3	33.16(0.61)		109.3	48.82(0.13)
	50.9	34.12(0.55)		129.3	48.29(0.12)
	52.1	35.35(0.49)		144.3	43.94(0.11)
	53.0	35.68(0.54)		193.3	40.12(0.11)
	54.2	35.20(0.60)		290.5	34.58(0.05)
	55.0	38.35(0.55)		388.0	28.55(0.11)
	56.2	38.72(0.62)		489.0	23.67(0.11)
	57.0	39.97(0.88)		687.0	19.95(0.06)
	58.2	40.74(0.65)		836.0	18.04(0.05)
	60.2	40.84(0.65)		985.0	15.81(0.04)
	61.3	42.79(0.67)	Ti^{2+}	21.8	−0.01(0.60)
	62.5	42.80(0.52)		23.0	0.35(0.46)
	64.1	43.90(0.66)		23.8	0.72(0.59)
	64.9	43.56(0.85)		24.7	1.81(0.59)
	66.0	41.42(0.44)		25.8	1.20(0.55)
	66.8	44.83(0.84)		26.6	0.85(0.60)
	68.4	43.56(0.50)		27.8	2.15(0.58)

TABLE I. (*Continued*).

Target	E (eV)	σ (10^{-18} cm^2)	Target	E (eV)	σ (10^{-18} cm^2)
Ti^{2+}	28.7	4.33(0.56)	Ti^{2+}	885.0	46.70(0.70)
	29.6	5.53(0.41)		1181.0	38.22(0.56)
	30.9	8.95(0.67)		1486.0	29.90(0.90)
	31.7	16.04(0.79)			
	32.9	24.98(0.96)	Fe^{2+}	15.4	0.67(0.65)
	33.7	31.06(1.11)		16.1	−1.23(0.62)
	34.8	39.11(0.81)		17.2	0.52(0.60)
	35.9	45.38(0.91)		19.0	0.56(0.62)
	38.1	51.60(1.00)		20.8	0.26(0.56)
	39.6	52.58(0.80)		21.9	1.70(0.63)
	40.8	54.30(1.00)		22.7	−0.12(0.50)
	41.7	56.00(1.00)		24.8	1.08(0.48)
	42.9	59.60(1.00)		26.0	2.22(0.65)
	43.7	63.00(0.70)		28.0	5.84(0.68)
	44.9	71.80(0.90)		29.8	8.20(0.70)
	45.8	76.90(0.80)		31.1	8.45(0.78)
	46.7	77.20(0.90)		31.9	11.04(0.69)
	48.0	78.10(0.70)		34.0	16.66(0.72)
	48.9	76.90(0.80)		36.1	21.79(0.76)
	50.0	74.70(0.90)		38.5	21.20(0.77)
	51.0	74.90(1.00)		40.5	23.13(0.71)
	52.0	76.21(0.74)		41.0	23.23(0.70)
	53.9	78.40(1.10)		42.2	24.12(0.78)
	55.0	80.10(1.40)		44.3	26.79(0.68)
	55.8	80.30(1.70)		45.7	29.62(0.53)
	57.9	81.60(1.70)		46.3	28.35(0.39)
	60.0	83.10(1.70)		48.3	31.01(0.49)
	61.9	85.20(1.80)		50.7	34.07(0.49)
	62.7	84.20(0.80)		52.2	36.05(0.72)
	63.8	84.30(1.80)		54.1	37.82(0.72)
	65.8	83.80(1.70)		55.8	41.10(0.73)
	66.5	85.70(1.80)		56.2	39.72(0.71)
	68.0	84.80(1.50)		58.2	43.55(0.78)
	69.3	86.60(2.50)		60.5	44.49(0.53)
	71.7	87.50(2.50)		62.2	46.60(0.76)
	72.7	89.30(1.90)		64.1	48.69(0.82)
	75.3	90.40(1.50)		65.9	48.81(0.56)
	80.1	92.80(1.50)		68.2	51.22(0.84)
	85.0	92.50(1.50)		70.5	51.83(0.54)
	89.9	91.70(1.50)		72.2	53.70(0.86)
	95.1	92.20(1.20)		75.6	54.11(0.71)
	100.0	92.20(1.40)		80.6	56.19(0.74)
	105.0	95.20(1.50)		85.5	56.25(0.75)
	110.0	95.40(1.50)		90.4	57.41(0.74)
	114.0	98.10(1.50)		95.3	58.93(0.43)
	119.5	96.90(1.10)		100.6	59.46(0.73)
	124.0	97.20(1.30)		115.0	62.60(0.86)
	129.0	94.80(1.50)		134.0	64.16(0.84)
	134.0	95.10(1.50)		144.0	65.29(0.87)
	144.0	92.50(1.90)		154.0	63.85(0.73)
	154.0	92.50(2.60)		174.0	63.90(0.77)
	183.0	90.20(2.50)		193.0	62.60(0.75)
	193.0	88.80(1.50)		242.0	62.24(0.72)
	213.0	87.90(2.50)		291.7	59.40(0.39)
	242.0	86.50(1.40)		390.0	50.22(0.52)
	272.0	80.60(2.30)		489.0	46.04(0.51)
	292.0	79.60(0.70)		687.0	40.72(0.45)
	390.0	68.30(0.90)		886.0	36.51(0.29)
	489.0	60.80(1.20)		1186.0	31.60(0.26)
	687.0	53.20(1.10)		1486.0	28.04(0.32)

The electron beam was chopped and the scalars appropriately gated to allow separate measurements of background and signal plus background. The difference between these scalar count rates is the net signal R. The cross section for electron-impact ionization of the incident ion at a collision velocity $v=(v_i^2+v_e^2)^{1/2}$ was determined using the relationship

$$\sigma=\frac{Rqe^2v_iv_eF}{I_iI_e(v_i^2+v_e^2)^{1/2}D}\ , \tag{2}$$

where v_i and v_e are the ion and electron velocities, q is the initial charge state of the ion, and D is the product of signal-ion transmission and detection efficiencies.

The electron gun used is patterned after one developed by Taylor *et al.*[5] which has been studied in detail. The relative energy spread in the measurements is about 1 eV FWHM, an estimate based on measurements[6] of electron-impact excitation of Al^{2+}

Ions were formed in the Oak Ridge National Laboratory Penning Ion Gauge source (ORNL-PIG), a cold-cathode Penning discharge source, which has been described elsewhere.[7] For the metal ions Ti^{2+} and Fe^{2+}, an arc was struck using a buffer gas of argon. Solid rods of Fe or Ti were fed through a small hole in the rear wall of the cylindrical anode. When CCl_4 was introduced into the discharge, it dissociated and metal chlorides with relatively high vapor pressures were formed by reaction of the hot metal rods with Cl atoms. The volatile chlorides entered the discharge, where the metal ions were produced by an unknown sequence of electron-impact dissociation and ionization. Thus, metal-ion beams of several tens of nanoamperes were obtained. To form Cl^{2+} beams, CCl_4 was mixed with the Ar buffer gas; and BF_3 was used to generate the F^{2+} beam. Again, ion beams of several tens of nanoamperes resulted.

III. RESULTS AND DISCUSSION

The measured cross sections are presently in Table I. The relative uncertainties as determined by the counting statistics are presented in parentheses and are one standard deviation of the mean. The error budget is presented in Table II. Uncertainties presented in this table are quoted at a "good" confidence level, estimated to be equivalent to a 90% statistical confidence level.

TABLE II. Experimental uncertainties at a "good" confidence level (CL) estimated to be equivalent to a 90% CL. Systematic uncertainties judged to have a possible correlation were added linearly after which a quadrature sum was made.

Source	Uncertainty (%)
Statistical uncertainty	
Typical value in % of peak value	±3
Systematic uncertainties	
Particle-counting efficiency	±3
Transmission to signal ion counter	±4
Background modulation	±1
Incident-ion current	±4
Incident-electron current	±3
Form-factor evaluation	±3
Uncertainty in velocities	±1
Total systematic	±8
Total % uncertainty (typical)	±9

A. $Ti^{2+}(1s^22s^22p^63s^23p^63d^2)$

The electron-impact single-ionization cross section for Ti^{2+} is presented in Fig. 2. The values are significantly larger than predicted by the Lotz semiempirical formula.[8] The situation for inner-shell ionization is similar to that for Ti^{3+} measured by Falk *et al.*[2] Removal of a $3p$ electron leaves the ion in a state which will autoionize two-thirds of the time[9,10] to form Ti^{4+}. To account for this fact the contribution of the $3p$ shell to the single-ionization cross section has been scaled by one-third in these predictions. The cross section rises sharply above threshold (27.85 eV) reaching a maximum value of 98×10^{-18} cm^2 near 114 eV. There is significant structure with the most distinct feature appearing near 47 eV. This bump, shown expanded in Fig. 3, has a full width at half maximum (FWHM) of just over 4 eV. The width of the rise at 45 eV may essentially be attributed to the 1-eV energy spread in the electron beam. We are not aware that such distinct features have been observed previously and are tempted to associate this one with resonant-recombination—double-autoionization,[11] i.e., $3p^63d^2+e\rightarrow3p^53d^3nl\rightarrow3p^63d+2e$. Another possibility is excitation to the $3p^53d^3$ autoionizing levels. However, we are unable to distinguish between these possibilities with the present experimental technique.

The magnitude of the disparity between Lotz formula calculations and experiment and the richness of the structure is reminiscent of the Ti^{3+} data of Falk *et al.*[2] While the magnitude of the enhancement to the cross section from excitation-autoionization is not as great in the present data, structures in the curve are more pronounced here. Pindzola *et al.*[10] have calculated excitation-autoionization contributions for Ti^{2+} in the distorted-

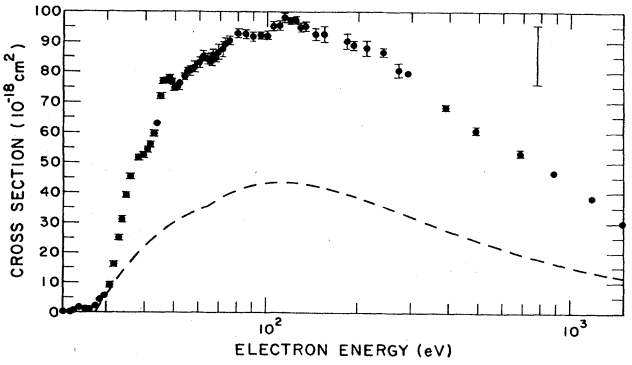

FIG. 2. Total cross section for $Ti^{2+}+e\rightarrow Ti^{3+}+2e$. Solid points, present experimental data; dashed curve, from Lotz semi-empirical formula (Ref. 8). Bars represent 1 standard deviation of mean and are statistical only. Bar at right represents total uncertainty (Table II) of peak value at a "good" confidence level.

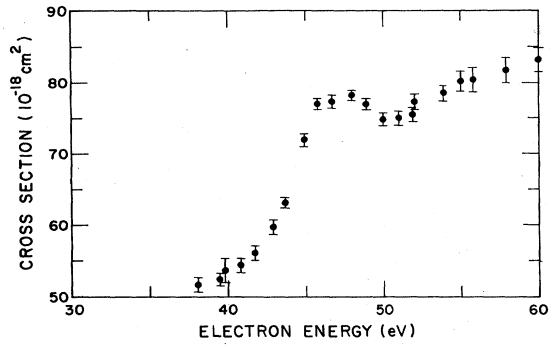

FIG. 3. Expanded view of Ti^{2+} data, showing the feature near 45 eV.

wave approximation. They treated the autoionizing levels both with an average-statistical model and a level-to-level basis. The two methods of treating the autoionizing levels give results in quite good agreement, since there are over 100 autoionizing levels within the $3p^5 3d^3$ configuration. Both theories predict a rapid change in the cross section from 30 to 35 eV followed by a 10-eV plateau, with further jumps in the cross section around 45 eV. Figure 2 shows that this qualitative behavior is observed experimentally; however, the calculated excitation-autoionization contributions are about a factor of 2 larger than observed. Pindzola *et al.*[10] note that they expect inclusion of configuration-interaction effects in the level-to-level distorted-wave calculations to lower the theoretical values and thus bring them into closer agreement with experiment.

The data presented here are in good agreement with recent unpublished data of Diserens *et al.*,[12] except the data here tend to be about 10% higher above 80 eV, and the feature near 47 eV is more pronounced here.

B. $Fe^{2+}(2s^2 2s^2 2p^6 3s^2 3p^6 3d^6)$

Figure 4 shows the ionization cross section for Fe^{2+}. Considerable ionization below the 34.8-eV ground-state threshold indicates a sizable metastable content in the ion beam. A predicted[10] enhancement near 57 eV due to excitation-autoionization processes does not appear in the experimental data, and as pointed out by Pindzola *et al.*[10] several factors may combine to produce the "masking" of the indirect contributions:

(1) the distorted-wave direct cross-section calculations probably overestimate the true direct process,

(2) the total $3p \rightarrow 3d$ collision strength for Fe ions is about $\frac{1}{6}$ that of Ti ions as estimated using the average-configuration distorted-wave approximation, and

(3) there are very many levels in both the final excited and ionized configuration which distribute the cross section gradually over energy.

The Lotz formula calculations,[8] distorted-wave calculations using Younger's parameters,[13] and the experimental data agree quite well at energies above 100 eV. Since the Auger process leads to multiple ionization when one has inner-shell ionization, it is believed that effectively only the $3d$ electrons contribute to single ionization, and this is the only shell included in the calculations presented here. Of course the large metastable content of the target beam complicates any comparisons with theory. Pindzola *et al.*[10] have reported calculations with target Fe^{2+} ions at a temperature corresponding to 20 eV, with results in better agreement with our experimental results than the simple curves shown in Fig. 4.

C. $F^{2+}(1s^2 2s^2 2p^3)$

Figure 5 shows the cross section versus electron energy for ionization of F^{2+}. The data rise smoothly from the threshold energy of 62.7 eV to a peak value of 18×10^{-18} cm^2 at a collision energy of 190 eV. The onset of direct ionization of $2s$ electrons at 79.4 eV does not noticeably enhance the total single-ionization cross section.

For comparison with experiment, predictions of the three-parameter Lotz formula[1] and distorted-wave with exchange (DWX) calculations of Younger[14] are presented as the dashed and solid curves, respectively. Younger's calculations and the measured values are in good agreement in this case, while the prediction obtained from the Lotz formula lies slightly below both of them. The two lowest-energy experimental points may be indicative of a small population of metastable ions in the target beam.

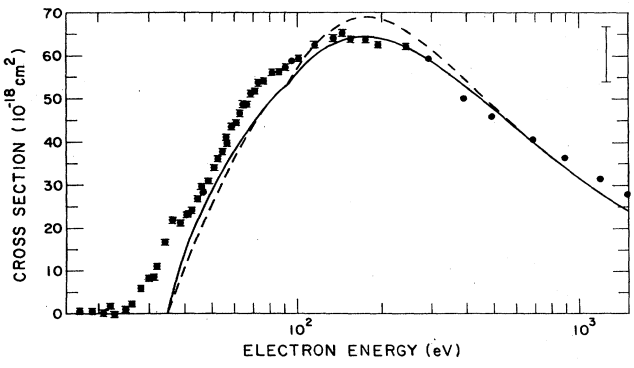

FIG. 4. Total cross section for $Fe^{2+} + e \rightarrow Fe^{3+} + 2e$. Solid points, present data; solid curve, distorted wave (Ref. 13); dashed curve, Lotz formula (Ref. 8). Uncertainties as in Fig. 2.

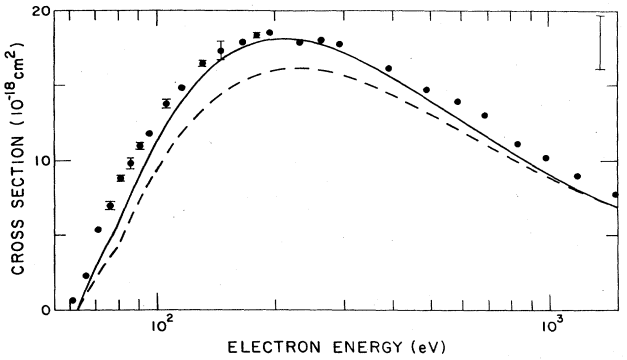

FIG. 5. Total cross section for $F^{2+} + e \rightarrow F^{3+} + 2e$. Notation as in Fig. 4; DW curve from Ref. 14.

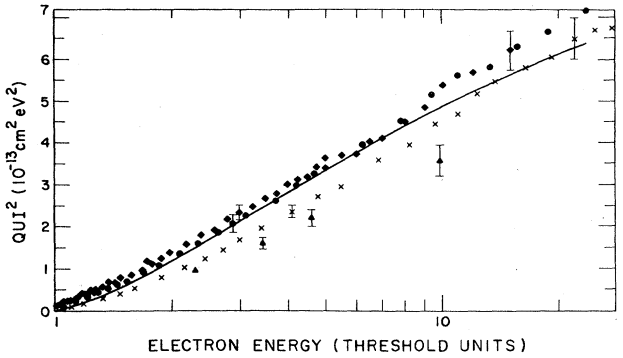

FIG. 6. "Bethe plot" of the product of scaled energy and scaled ionization cross section, QUI^2, vs $\log U$ for the nitrogen-like isoelectronic sequence. Included are ●, the present (Fig. 5) F^{2+} data; ×, the O^+ data of Aitken and Harrison (Ref. 16); ▲, the O^+ measurements of Müller *et al.* (Ref. 17); and ◆, the Ne^{3+} data of Gregory *et al.* (Ref. 15). Solid line is the distorted-wave calculation of Younger (Ref. 14) for F^{2+}.

To compare cross sections for different members of the nitrogen isoelectronic sequence, the scaled cross section $UI^2\sigma$, where U is the energy in threshold units and I is the ionization potential of the species, is plotted versus $\log U$ (a Bethe plot) in Fig. 6. This figure shows remarkable similarity between the data[15] for Ne^{3+} and the present F^{2+} data. In fact, cross sections for the two species are indistinguishable when plotted in this way. The solid curve represents scaled cross sections for F^{2+} calculated for direct ionization using parameters provided by Younger.[14] The scaled O^+ data of Aitken and Harrison[16] and those of Müller *et al.*[17] lie slightly lower, but above $U=2$ have similar slope to the F^{2+} and Ne^{3+} data. Above ten threshold units the data measured for all three species show a slight increase in scaled cross sections relative to the theoretical F^{2+} curve.

D. $Cl^{2+}(1s^22s^22p^63s^23p^3)$

The single-ionization cross-section data for Cl^{2+} presented in Fig. 7 rise sharply from the threshold at 39.7 eV to a peak value of 47×10^{-18} cm^2 near 80 eV. Structure appears near 100 eV which is slightly sharper than

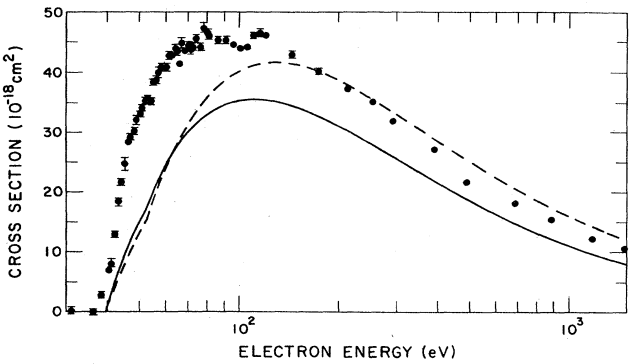

FIG. 7. Total cross section for $Cl^{2+}+e\rightarrow Cl^{3+}+2e$. Notation as in Fig. 4; DW curve from Ref. 14.

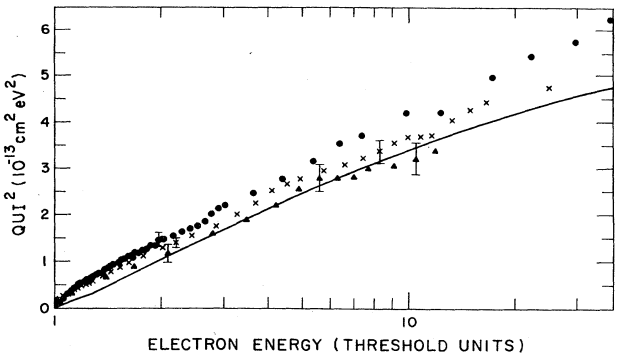

FIG. 8. Bethe plot as in Fig. 6 for phosphorouslike ions. Included are ●, the current Cl^{2+} data; ×, Ar^{3+} data of Gregory *et al.* (Ref. 15); ▲, the Ar^{3+} data of Müller *et al.* (Ref. 17). Solid curve is the Ar^{3+} DWX calculation of Younger (Ref. 14).

the similar feature in its isoelectronic neighbor Ar^{3+} (Ref. 15). In the Ar^{3+} the analogous feature appears near 180 eV and is attributed to $2p$-nl inner shell excitation-autoionization and that interpretation is reasonable here as well. The dashed curve is the cross section predicted using the semiempirical formula of Lotz, and it is lower than the experimental curve up to 150 eV and slightly higher above 400 eV. In contrast, however, Younger's DWX calculations[14] lie below both the Lotz formula prediction and the experimental data. Since direct ionization of electrons in the $2p$ and lower shells leaves the ion in an autoionizing configuration which would most often lead to double ionization, only contributions from the $3p$ and $3s$ shells have been included in the predictions shown in these figures. The sharp rise just above threshold can probably be attributed to indirect processes (e.g., excitation-autoionization) which significantly enhance the total ionization cross section in this region. As in the work[15] on Ar^{3+} this can most likely be attributed to excitation of inner-shell $3s$ electrons to autoionizing states. Again, there is only meager evidence of contributions to the ionization cross section from metastable ions in the target beam.

Figure 8 is a Bethe plot of the scaled ionization cross section versus $\log U$ above threshold for the isoelectronic neighbors Cl^{2+} and Ar^{3+}. Also displayed as the solid curve is a scaled version of Younger's[14] DWX calculation for Cl^{2+}. The Cl^{2+} and Ar^{3+} cross sections are very similar but deviate from each other slightly at energies greater than $U=2$. Because of the indirect processes discussed above, these cross sections do not follow the simple DWX curve as was the case for F^{2+} and Ne^{3+} shown in Fig. 6.

E. $Ar^{2+}(1s^22s^22p^63s^23p^4)$

Figure 9 is a plot of the Ar^{2+} ionization cross section including present measurements and those of Müller *et al.*[17] Also included for comparison are curves based upon distorted-wave calculations using parameters provided by Younger[12] and upon the Lotz formula.[1] Below 60 eV the data of Müller *et al.* agree quite well with present

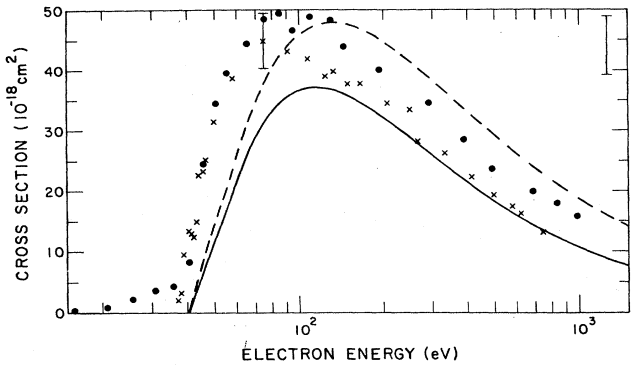

FIG. 9. Total cross section for $Ar^{2+}+e \rightarrow Ar^{3+}+2e$. Notation as in Fig. 4. $\times$, Müller *et al.* (Ref. 17). Relative uncertainties are comparable to the size of the solid circles, and are thus not shown.

measurements. At higher collisional energies the present data are consistently higher than those of Müller *et al.* Similar patterns show up in other comparisons of data; for example, the data of Müller *et al.* for Ar^{3+} are lower at high energies than those of Gregory *et al.*[15] (see Fig. 8), and their data for O^+ are lower than those of Aitken and Harrison.[16] It is unclear what systematic differences there are between the experiments. In comparing the measurements with predictions at energies below 80 eV, both calculations underestimate the ionization cross section. This fact, together with the rise which is much sharper than that of the theories that include only direct processes, indicates a significant contribution to the cross section from indirect processes. The presence of nonzero cross sections below the ground-state ionization energy of 42.6 eV indicates a metastable component of the beam. In this case, some metastable states which lie as much as 20 eV above the ground state must be populated. No attempt was made to vary the metastable fraction of the beam to quantify[18] a separation of the ground-state cross section.

IV. CONCLUSIONS AND COMMENTS

Measurements have been made and presented here of cross sections for electron-impact ionization of several doubly-charged ions, Ti^{2+}, Fe^{2+}, F^{2+}, Cl^{2+}, and Ar^{2+}. Data for F^{2+} are in good agreement with distorted-wave calculations, and also agree with scaled measurements on the isoelectronic ions O^+ and Ne^{3+}. Measurements for Cl^{2+}, on the other hand, indicate substantial contributions to the cross section from excitation-autoionization. These lead to differences at low energies of about a factor of 2 between measured cross sections and those obtained using direct processes calculations. There is agreement between the scaled cross sections for Cl^{2+} and those of the isoelectronic ion Ar^{3+}, and similar enhancement by indirect processes is observed at low energies in both cross-section curves.

The measured cross sections for Ti^{2+} are again significantly larger than those calculated for direct ionization, and large contributions from excitation-autoionization are thought to be responsible. Unusual structure in the cross-section curve near 45 eV is narrow enough so that we speculate that resonant-recombination—double-autoionization has a role in this feature; simple excitation-autoionization would not be expected to fall so rapidly above its threshold, unless it were strongly dominated by spin-forbidden transitions.

For Fe^{2+} and Ar^{2+} ions, there are significant fractions of metastable ions in the target beams leading to substantial apparent cross sections below the threshold for ground-state ionization. Since the ions are obtained from a plasma source, these apparent cross sections are probably appropriate for plasma modeling. No attempt was made to separate the ground-state cross sections. In the Fe^{2+} data, anticipated contributions from excitation-autoionization were not observed, and the possible reasons are discussed.

ACKNOWLEDGMENTS

The authors acknowledge valuable conversations with R. Phaneuf, M. Pindzola, D. Griffin, and C. Bottcher. They also thank S. Younger for providing unpublished, distorted-wave data for F^{2+} and Cl^{2+} and D. Griffin for calculating inner-shell ionization energies. Thanks are due J. W. Hale for technical assistance with the ion source. This work was sponsored in part by the Office of Fusion Energy, U.S. Department of Energy.

APPENDIX: IONIZATION RATE COEFFICIENTS

Ionization rate coefficients were calculated for the ions discussed in this paper using a technique of curve fitting to the cross-section data similar to that discussed by Crandall *et al.*[19] An example of the rate coefficients so calculated are shown for Ti^{2+} in Fig. 10. To obtain the rate coefficient $S(T)$ for any of the ions at temperatures $10^4 \leq T \leq 10^7$, the rate coefficients are expanded by Chebyshev polynomials of the first kind, $T_r(x)$. The expansion coefficients are presented in Table III.

The expansion can be written

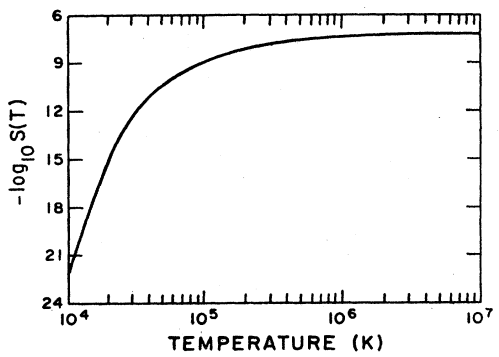

FIG. 10. $-\log_{10}S(T)$ vs T for Ti^{2+} resulting from cross-section measurements reported here.

TABLE III. Expansion coefficients for generating ionization rate coefficients using Eqs. (4) and (5) for interval $10^4 \leq T \leq 10^7$ K. [Parameters for Ar^{2+} and Fe^{2+} are for the target ion beams which included metastables. For the cases presented here, (b_0-b_2) has been evaluated using both the seven-place accuracy in the a_i quoted here and three-place accuracy. Results were identical to within 1%.] Numbers in parentheses signify factors of powers of 10.

Ion	F^{2+}	Cl^{2+}	Ar^{2+}	Fe^{2+}	Ti^{2+}
a_0	3.727 782(−11)	6.742 667(−11)	2.496 739(−11)	6.884 292(−11)	1.397 098(−10)
a_1	−1.238 792(−11)	−1.608 921(−11)	6.449 460(−12)	−5.250 469(−12)	−3.329 816(−11)
a_2	4.707 810(−13)	−1.745 272(−11)	−8.351 721(−12)	−8.200 637(−12)	−1.941 413(−11)
a_3	−2.315 241(−12)	8.191 805(−12)	−5.647 509(−12)	−4.383 913(−12)	4.620 821(−12)
a_4	1.897 906(−12)	1.943 982(−12)	3.319 693(−12)	2.663 895(−12)	3.643 723(−12)
a_5	−7.407 936(−13)	−2.792 451(−12)	1.989 570(−12)	7.110 386(−13)	−3.453 378(−12)
a_6	2.433 800(−13)	9.842 638(−13)	−1.329 050(−12)	−1.751 0.96(−13)	1.909 593(−12)
a_7		1.762 070(−13)	−6.075 336(−13)	−2.966 321(−13)	−1.186 652(−13)
a_8		−4.223 417(−13)	6.662 119(−13)		−3.422 202(−13)
a_9		1.800 748(−13)	1.118 225(−13)		
a_{10}			−2.333 013(−13)		
I_e (eV)	62.7	39.7	15.90	24.80	27.8

$$S(T)=T^{1/2}e^{-I_e/kT}\left[a_0/2+\sum_{r=1}^{n}a_rT_r(x)\right], \tag{A1}$$

where $x=(\log T-5.5)/1.5$ for the temperature interval $10^4 \leq T \leq 10^7$, T is temperature in kelvin, and I_e is the effective ionization energy for the target ions.

Rather than evaluating the Chebyshev polynomials, the rate coefficients are most easily generated from the a_r using Clenshaw's[20] algorithm

$$\begin{aligned} &b_{n+2}=b_{n+1}=0\,,\\ &b_r=2xb_{r+1}-b_{r+2}+a_r,\quad r=n,n-1,\ldots,0\\ &S(T)=\tfrac{1}{2}T^{1/2}e^{-I_e/kT}(b_0-b_2)\,. \end{aligned} \tag{A2}$$

The b_r's are most readily calculated sequentially from the algorithm, starting with $b_n=a_n$ and progressing downward. However, the single polynomial also results:

$$\begin{aligned} (b_0-b_2)=&1024a_{10}x^{10}+512a_9x^9+(256a_8-2560a_{10})x^8+(128a_7-1152a_9)x^7+(64a_6-512a_8+2240a_{10})x^6\\ &+(32a_5-224a_7+864a_9)x^5+(16a_4-96a_6+320a_8-800a_{10})x^4+(8a_3-40a_5+112a_7-240a_9)x^3\\ &+(4a_2-16a_4+36a_6-64a_8+100a_{10})x^2+(2a_1-6a_3+10a_5-14a_7+18a_9)x\\ &+(a_0-2a_2+2a_4-2a_6+2a_8-2a_{10})\,, \end{aligned} \tag{A3}$$

and this can be readily applied if the user prefers.

*On leave from Physics Department, Wesleyan University, Middletown, CT 06457.

†Present address: Division of Magnetic Fusion Energy, U. S. Department of Energy, Washington, D. C. 20545.

[1]W. Lotz, Z. Phys. **216**, 241 (1968).

[2]R. A. Falk, G. H. Dunn, D. C. Gregory, and D. H. Crandall, Phys. Rev. A **27**, 762 (1983).

[3]A. Lorenz, in the proceedings of the first meeting of the International Fusion Research Council (IFRC) Subcommittee on Atomic and Molecular (A&M) Data for Fusion, International Atomic Energy Agency Report No. INDC (SEC)-77/GA, 1981 (unpublished).

[4]D. H. Crandall, R. A. Phaneuf, and P. O. Taylor, Phys. Rev. A **18**, 1911 (1978).

[5]P. O. Taylor, K. T. Dolder, W. E. Kauppila, and G. H. Dunn, Rev. Sci. Instrum. **45**, 538 (1974).

[6]D. S. Belić, R. A. Falk, G. H. Dunn, D. Gregory, C. Cisneros, and D. H. Crandall, Bull. Am. Phys. Soc. **26**, 1315 (1981).

[7]M. L. Mallory and D. H. Crandall, IEEE Trans. Nucl. Sci. **NS-23**, 1069 (1976).

[8]W. Lotz, Z. Phys. **220**, 466 (1969).

[9]C. Bottcher, D. C. Griffin, and M. S. Pindzola, J. Phys. B **16**, L65 (1983).

[10]M. S. Pindzola, D. C. Griffin, C. Bottcher, D. C. Gregory, A. M. Howald, R. A. Phaneuf, D. H. Crandall, G. H. Dunn, D. W. Mueller, and T. J. Morgan, Oak Ridge National Laboratory Report No. ORNL/TM-9436, 1985 (unpublished).

[11]K. J. LaGattuta and Y. Hahn, Phys. Rev. A **24**, 2273 (1981).

[12]M. J. Diserens, M. F. A. Harrison, and A. C. H. Smith (private communication).

[13]S. M. Younger, At. Data Fusion **7**, 190 (1981). A bulletin from the Controlled Fusion Atomic Data Center of Oak Ridge National Laboratory and the National Bureau of Standards.

[14]S. M. Younger (private communication).

[15]D. C. Gregory, P. F. Dittner, and D. H. Crandall, Phys. Rev.

A **27**, 724 (1983).
[16]K. L. Aitken and M. F. A. Harrison, J. Phys. B **4**, 1176 (1971).
[17]A. Müller, E. Salzborn, R. Frodl, R. Becker, H. Klein, and H. Winter, J. Phys. B **13**, 1877 (1980).
[18]R. A. Falk, G. Stefani, R. Camilloni, G. H. Dunn, R. A. Phaneuf, D. C. Gregory, and D. H. Crandall, Phys. Rev. A **28**, 91 (1983).
[19]D. H. Crandall, G. H. Dunn, A. Gallagher, D. G. Hummer, C. V. Kunasz, D. Leep, and P. O. Taylor, Astrophys. J. **191**, 789 (1974).
[20]C. W. Clenshaw, Math. Tables Comput. **9**, 118 (1955).